J. Fluid Mech. (1972), *vol.* 53, *part* 3, *pp.* 451–467
Printed in Great Britain

Some measurements of the distortion of turbulence approaching a two-dimensional bluff body

By P. W. BEARMAN
Department of Aeronautics, Imperial College, London

(Received 13 November 1971)

This paper describes an experimental study of the distortion of grid-generated turbulence as it approaches the stagnation region of a two-dimensional bluff body. When $L_x/D \gg 1$, where L_x is the scale of turbulence and D is a typical body dimension, along the mean stagnation streamline $(\overline{u^2})^{\frac{1}{2}}$ attenuates like the mean flow, whereas if $L_x/D \ll 1$ the turbulence is distorted by the mean flow field and $(\overline{u^2})^{\frac{1}{2}}$ will amplify because of vortex stretching. When $L_x/D = O(1)$ there is found to be a combination of these effects with attenuation of energy at low wavenumbers and amplification at high wavenumbers. Measurements of the pressure fluctuations at the stagnation point show that at low wavenumbers the level of the pressure fluctuations can be predicted by a direct application of Bernoulli's equation.

1. Introduction

When a bluff body is placed in a turbulent shear flow, for example a building in the earth's boundary layer, there will be some complex interaction between the mean flow field around the body and the approaching stream turbulence. This interaction will influence the relationship between upstream velocity fluctuations and the resulting pressure fluctuations on the body surface. The aim of the research described in this paper was to study experimentally the passage of grid-generated turbulence approaching the stagnation region of a two-dimensional body. Although this is a simpler problem than that posed above it retains the important feature of turbulence distortion.

Hunt (1971*a*) (see also Hunt 1971*b*) has formulated a theory, based on the rapid distortion theory of Batchelor & Proudman (1954), for analysing the distortion of turbulence in a flow sweeping past a body. The principal assumption made in the theory is that, in the time it takes for the turbulence to be swept past the body, the changes in the mean flow around the body and the effects of its boundaries distort the turbulence far more than its own internal viscous and nonlinear inertial forces. The turbulence will be distorted by the stretching and rotating of vortex line filaments as they are convected past the body. The assumptions made in rapid distortion theory are first, that the mean flow is irrotational and second, that $(\overline{u^2})^{\frac{1}{2}}/U \ll 1$ (where $(\overline{u^2})^{\frac{1}{2}}$ is the root-mean-square value of the longitudinal component of the turbulence and U is the mean velocity), so that the dominant contribution to the distortion comes from changes

in the mean flow and not from the turbulence itself. The neglect of viscous effects is justified if the distortion takes place in such a short time that the viscous decay of energy is very small. Batchelor & Proudman (1954) suggested the criterion

$$t - t' \ll [L_x/(\overline{u^2})^{\frac{1}{2}}]_{t=t'},$$

where t' is the time at the beginning of the distortion and L_x is the integral scale length in the mean flow direction of the longitudinal component of turbulence, say. For the flow past a body

$$t - t' = O(U_0/D),$$

where U_0 is free-stream velocity and D is a typical body dimension. This leads to the third condition that

$$(\overline{u_0^2})^{\frac{1}{2}}/U_0 \ll L_x/D.$$

Using these three assumptions Hunt (1971*a*) treated the problem of initially isotropic turbulence convected past a circular cylinder. Although the theory of Hunt will not be used directly the interpretation of the experimental results presented in this paper draws heavily on the basic ideas underlying this theory.

The flow along the stagnation streamline approaching a two-dimensional flat plate placed normal to the flow was investigated; along this line the turbulence is only subjected to plane strain. Experimental work on uniform plane strain has been carried out by several investigators, including Townsend (1954) and Tucker & Reynolds (1968), in suitably shaped distorting ducts. These experiments are unsatisfactory in the sense that the condition $(\overline{u^2})^{\frac{1}{2}}/U \ll L_x/D$ (where D is now some duct dimension) is not met. Tucker & Reynolds, however, have made suitable allowance for viscous decay in the analysis of their results. In some respects the external flow around bodies is more suited to a rapid distortion treatment, although there are regions of the flow, especially very close to the stagnation point, where the conditions of the theory are not satisfied. Along the stagnation streamline there is some balance between the distortion created by the modification to the vorticity field by the mean flow, which will increase $(\overline{u^2})^{\frac{1}{2}}$, and the effect of the boundary condition, that there can be no velocity normal to the body surface, which will reduce $(\overline{u^2})^{\frac{1}{2}}$. The experiments described in this paper were performed for four values of the turbulence scale in the range where this scale is of the same order as the size of the body.

The phenomenum of increased turbulence ahead of stagnation was first noted by Piercy & Richardson (1930) in some measurements ahead of an aerofoil in a wind tunnel with a high background turbulence level. Further mention is made by Keuthe, Willmarth & Crocker (1959), who examined the stagnation region on bodies of revolution. Work has been carried out by Sutera, Maeder & Kestin (1963) and by Sutera (1965) on the role of vorticity amplification in stagnation flow. They have examined theoretically a simple form of spatially varying sinusoidal pattern of vorticity, favourably orientated to produce stretching, entering a stagnation-point boundary layer. They find a neutral scale length for which amplification by stretching is exactly balanced by viscous dissipation. This theory has been extended by Sadeh, Sutera & Maeder (1970*a*, *b*) to the outer flow field for a similar form of vorticity distribution. Their theory does

Grid	Mesh size M (cm)	Bar size b (cm)	Distance to stagnation point, x/M
A	3·81	0·98	70·4
B	7·62	1·28	35·1
C	15·22	3·11	17·6
D	22·83	3·77	11·7

TABLE 1

not, however, allow for the important effect of the upstream influence of the condition that there can be no velocity normal to the body surface. Their theory is only valid, therefore, at very high wavenumbers. They compare their theory with some measurements in a turbulent flow approaching a plate where $L_x/D \ll 1$. This increased turbulence level due to the inviscid amplification of approaching turbulence should not be confused with the stagnation-point instabilities investigated by Kestin & Wood (1970).

In addition to the investigation of the turbulent velocity field, measurements of pressure fluctuations at the stagnation point are presented. These were made in order to determine the relationship between approaching velocity fluctuations and resulting pressure fluctuations, and to examine the dependence of this relationship on the scale parameter L_x/D. Marshall (1968) has completed a similar programme of measurements on a grid-generated turbulent flow approaching a disk. His measurements, however, were restricted to only one value of the turbulence scale.

2. Experimental arrangement

The experiments were conducted at the National Physical Laboratory in a wind tunnel with a 3 by 3 ft, 15 ft long working section. The tunnel is of the closed-return type and when empty has a free-stream turbulence level of better than 0·07 % and a maximum speed of about 150 ft/s. Highly turbulent flow was generated by the installation of square mesh grids at the beginning of the working section. Details of the grids, which were constructed of bars of rectangular cross-section, are given in table 1. The wind tunnel was equipped with a fine-pitch fan designed to operate unstalled with a high solidity grid in the working section.

The bluff body used was a flat plate spanning the tunnel and mounted normal to the flow. Of prime interest was the distortion of the approaching turbulence and in order to remove any unsteadiness in the flow around the plate, generated by vortex shedding in the wake, it was decided to fill in the wake along the theoretical free streamlines. The profile shape of the resulting body was designed according to Roshko's (1954) notched hodograph method. Details of the design of the model are given in the appendix. The model cross-section is shown in figure 1 and the size of the equivalent flat plate, D, is 2·54 cm. The model side faces become parallel in a distance of just less that D and remain parallel for $10D$. The body is terminated in a streamlined tail fairing length $6D$. Surface oil flow patterns showed there to be a region of separated flow situated towards the end

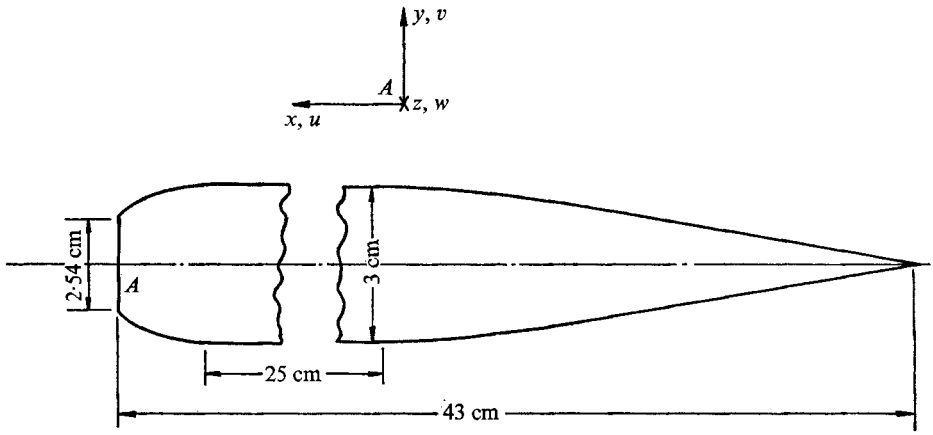

FIGURE 1. Flat-plate free-streamline model.

of the curved portion of the 'free streamline'. Trip wires were fitted at about $0{\cdot}5D$ from the 'edges' of the plate and removed the unwanted separations.

Turbulence measurements were made with Disa constant-temperature linearized hot-wire anemometers. A traverse gear was embedded in the model and either normal-wire or X-wire probes could be traversed out along the mean stagnation streamline. The hot-wire probe came out of the face of the model through an air-tight seal. In addition to the velocity measurements, fluctuating surface pressure measurements on the stagnation line were made using a $\frac{1}{2}$ in. Bruel & Kjaer microphone. The microphone was connected to a surface hole by about 1·3 cm of 2 mm probe tubing. The frequency response of the microphone and probe tube was checked against a standard Bruel & Kjaer microphone. Some damping had to be added to the probe tube to suppress the effect of the lowest resonant frequency; with damping the frequency response was made acceptably flat to 2 kHz. At frequencies less than about 20 Hz the level of power spectral densities had to be raised to compensate for a fall off in microphone response. Fluctuating velocity and pressure signals were recorded on a tape recorder for later digitization and analysis on a computer.

3. Experimental results

Flow behind the turbulence producing grids

The turbulence structure behind the four grids was investigated on the centre-line of the working section, in the absence of the model, at a distance from the grids corresponding to the distance to the stagnation point. The measurements of the intensity of the three components of the turbulence together with a representative value of scale, the longitudinal integral scale of the along wind component, are presented in table 2. The measurements were made at a wind speed of about 18 m/s and values of the grid Reynolds number R_m, based on mesh size, are given in table 2. In accordance with the results of other investigators, the turbulence components normal to the mean wind direction were found to be smaller than the along wind components. The values of the turbulence

Grid	$[(\overline{u^2})^{\frac{1}{2}}/U] \times 10^2$	$[(\overline{v^2})^{\frac{1}{2}}/U] \times 10^2$	$[(\overline{w^2})^{\frac{1}{2}}/U] \times 10^2$	L_x (cm)	L_x/D	$R_m \times 10^{-4}$
A	2·09	1·63	1·66	3·05	1·2	4·7
B	2·83	2·2	2·34	4·57	1·8	9·5
C	5·71	4·4	4·81	6·54	2·57	18·9
D	6·40	4·95	5·31	6·05	2·38	28·4

TABLE 2

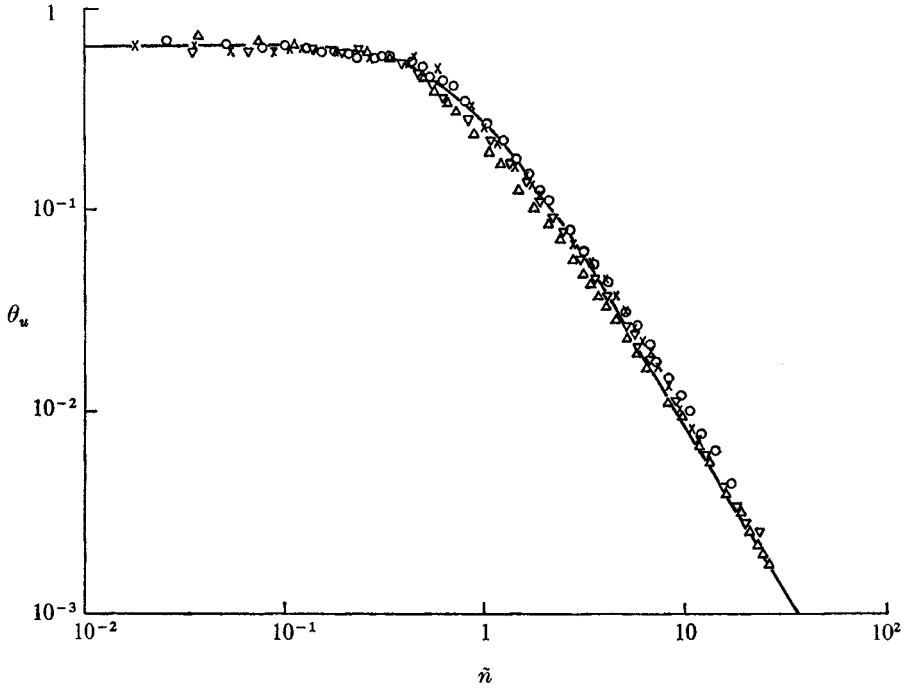

FIGURE 2. Spectra of the u component in the absence of the model. ×, grid A; ○, grid B; △, grid C; ▽, grid D; ——, von Kármán spectrum.

scale were estimated from power spectral density measurements, assuming Taylor's hypothesis. The scale produced by the smaller mesh grid, grid C, is larger than that produced by grid D. This is because scale increases with distance from a grid and the measuring station was comparatively nearer to the grid in case D.

Spectra measurements were made of the u component of turbulence for the flow behind each of the grids. Figure 2 shows the spectra plotted in a normalized form. The power spectral density $F(n)$ is plotted in the non-dimensional form $(F(n)\,U_0)/(2\pi L_x \overline{u_0^2}) = \theta_u$ against the frequency parameter $(2\pi n L_x)/U_0 = \tilde{n}$, where n is frequency in Hz. The results are shown compared with the spectrum calculated from von Kármán's interpolation formula (see Hinze 1959). This spectrum has the form $\theta_u = (2/\pi)\,[1+1{\cdot}8\tilde{n}^2)^{-\frac{5}{6}}$ and gives a good representation of the ex erimental results.

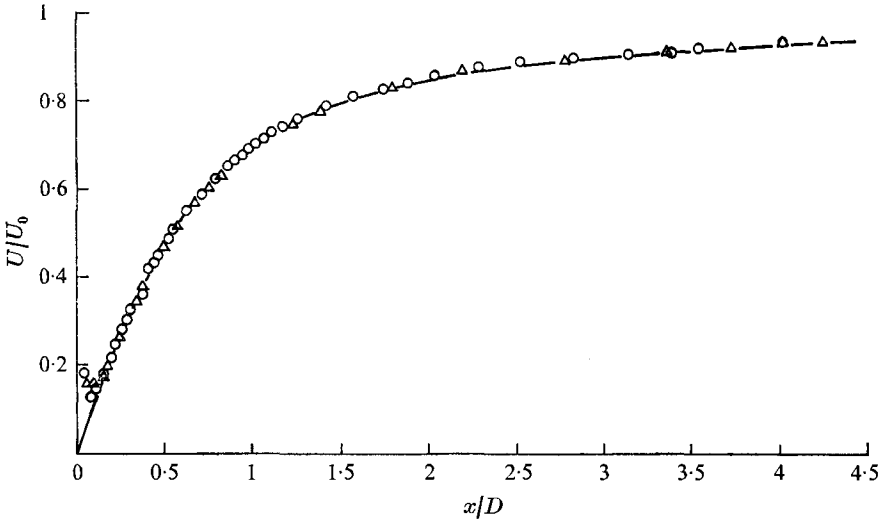

FIGURE 3. Mean velocity approaching stagnation. ○, smooth flow; △, grid D; ——, hodograph solution.

Velocity measurements ahead of the body

The first measurements were made in smooth flow and the mean velocity profile along the stagnation streamline is shown in figure 3. The hot wire was traversed out to just over 4 plate widths ahead of the model. Within a distance of $0{\cdot}1D$ from the surface the hot-wire results were subject to a number of errors, the most serious of which was that the seal at the stagnation point could not be held when the wire was very close to the surface. Also the presence of the wire may have moved the stagnation point slightly. Either of these effects could have caused the apparent small increase in velocity measured very close to the surface. As a check on the measuring technique the velocity distribution was compared with that predicted by Roshko's (1954) hodograph method. Details of the computation of the velocity field are given in the appendix. The predicted profile is also shown in figure 3 and the agreement with experiment is seen to be good. In turbulent flow the mean velocity profile was measured in the flow behind each of the four grids and showed good agreement with the smooth-flow result. The velocity profile measured with grid D in the tunnel is shown in figure 3. Hiemenz's solution for the boundary layer at the stagnation point gives a thickness of just over $0{\cdot}01D$. All the measurements were made well outside this boundary-layer region.

Although not strictly part of this investigation, turbulence measurements with a normal wire were made ahead of the body in smooth flow and showed a number of unusual features. It is to be expected that the turbulence intensity based on local velocity might gradually rise as the model is approached. However there were several local regions of increased turbulence level along the stagnation streamline, one as high as 1 % at $x/D = 0{\cdot}35$, which appear to have been caused by the presence of the hot wire in the flow. The wire was situated in a region of strong adverse pressure gradient and it may well have had some disturbing effect on the flow. If the wire was moved slightly off the stagnation streamline

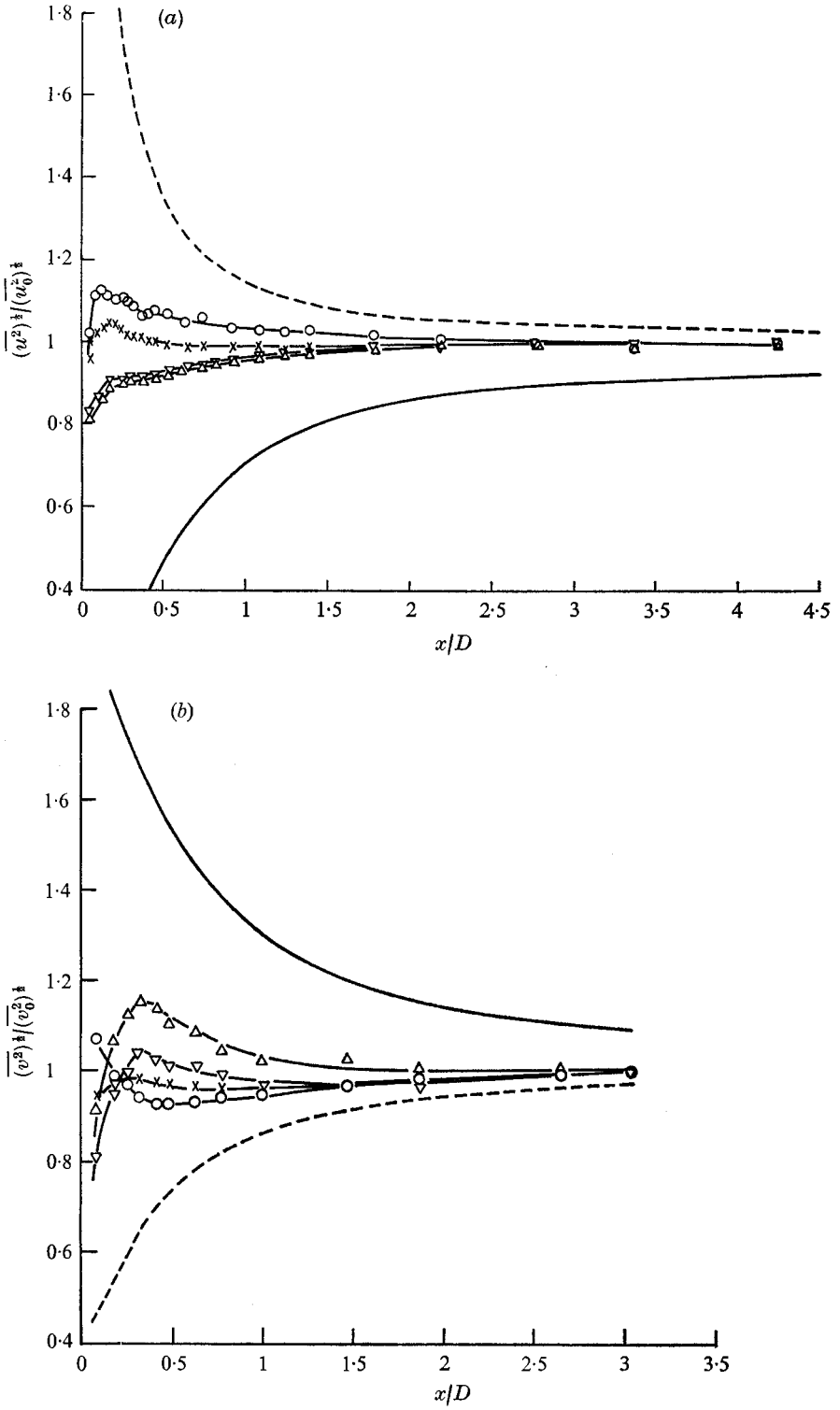

FIGURES 4(*a*) and (*b*). For legend see following page.

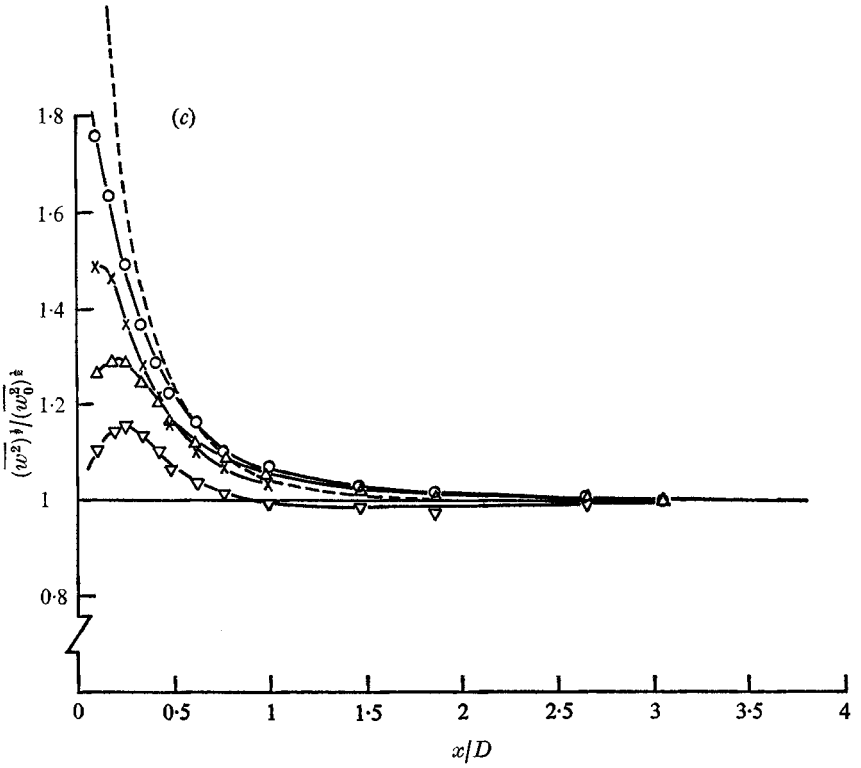

FIGURE 4. Velocity component approaching stagnation. ○, grid A; ×, grid B; △, grid C; ▽, grid D; – – –, $L_x/D = 0$; ——, $L_x/D = \infty$. (*a*) u component. (*b*) v component. (*c*) w component.

the disturbance disappeared. Measurements in turbulent flow, on the other hand, showed no obvious evidence of any interference by the hot-wire probe.

The root-mean-square values of all three components of turbulence were measured ahead of the body along the stagnation streamline. It is difficult to interpret their meaning if they are simply plotted as a variation of local turbulence intensity because the changes in intensity are dominated by the changes in the mean velocity. Instead the local root-mean-square value of the turbulence component has been divided by its value recorded at $x/D = 4{\cdot}25$. Figure 4(*a*) shows the variation of $\overline{(u^2)^{\frac{1}{2}}}/\overline{(u_0^2)^{\frac{1}{2}}}$ ahead of stagnation for the four values of scale tested. The two smaller scales show an amplification of energy, whereas the two larger scales show a continuous attentuation. At the surface, of course, the value of $\overline{(u^2)^{\frac{1}{2}}}/\overline{(u_0^2)^{\frac{1}{2}}}$ must drop to zero. There will be some natural decay of turbulence between $x/D = 4{\cdot}25$ and 0. Without the model in position the turbulence was found to decay by only about 2–3 % in this distance and no attempt has been made to correct the results. These results show similar features to some measurements by Petty (see Hunt 1971*b*) of the variation of the u component in turbulent flow approaching a circular cylinder.

Very near the stagnation point the hot wire can only give a rough indication of the level of the fluctuating velocities because of the very high local turbulence

Grid	Maximum $(\overline{u^2})^{\frac{1}{2}}/U$	Amplification of intensity
A	0·18	8·6
B	0·21	7·43
C	0·32	5·60
D	0·34	5·31

TABLE 3

intensities. The hot-wire output was linearized but further errors will arise at high levels of turbulence owing to the nonlinear yaw response. This effect is likely to be more pronounced for the X-probe, for which there is the strong possibility that part of the time the instantaneous velocity vector may be at an angle of more than 45° to the free-stream direction. Table 3 shows the highest values of local intensity recorded and in all cases this occurred at $x/D = 0{\cdot}1$. Grid *A* showed a nearly ninefold increase in the value of intensity.

The other component of turbulence in the plane containing the cross-section of the model, $(\overline{v^2})^{\frac{1}{2}}/(\overline{v_0^2})^{\frac{1}{2}}$, is shown in figure 4(*b*). The system of axes is shown in figure 1. The third component $(\overline{w^2})^{\frac{1}{2}}/(\overline{w_0^2})^{\frac{1}{2}}$, which is in a direction parallel to the stagnation line along the model, is plotted in figure 4(*c*). While $(\overline{v^2})^{\frac{1}{2}}/(\overline{v_0^2})^{\frac{1}{2}}$ shows generally an opposite effect to that of $(\overline{u^2})^{\frac{1}{2}}/(\overline{u_0^2})^{\frac{1}{2}}$, $(\overline{w^2})/(\overline{w_0^2})^{\frac{1}{2}}$ shows only amplification. Near the surface viscous effects will reduce these components to zero. Further discussion of these results is left until §4.

Power spectral density measurements ahead of the body

For each grid, power spectral densities of the longitudinal component of turbulence were computed at $x/D = 3{\cdot}025$, 0·624 and 0·183. The spectra measured at $x/D = 3{\cdot}025$ showed no significant variation from those measured in the absence of the model. The spectra measured at $x/D = 0{\cdot}624$ and 0·183 are shown in figures 5(*a*) and (*b*) respectively. Spectra are shown plotted as

$$(F(n)\,U_0)/(2\pi L_x \overline{u_0^2}) = \theta_u \quad \text{against} \quad (2\pi n L_x)/U_0 = \tilde{n},$$

and the area beneath each spectrum is $\overline{u^2}/\overline{u_0^2}$, i.e. the square of the ratio shown in figure 4(*a*). In order to compare these with the spectra measured in the absence of the body the curve obtained from the von Kármán interpolation formula is also shown.

Figure 5(*a*) shows that the power at low wavenumbers begins to decrease (or remain constant, grid *A*) and the largest attenuation occurs for the flow with the largest scale, grid *C*. At higher wavenumbers the turbulence from all grids shows an increase in power. In figure 5(*b*) the apparent shift of energy from low wavenumbers to higher wavenumbers is more marked, while at the high wavenumber end of the spectrum viscous decay of energy causes the spectra to fall off at a rate greater than $-\frac{5}{3}$. It is interesting to note that for grid *A*, giving the smallest scale, the turbulence amplified even at low wavenumbers.

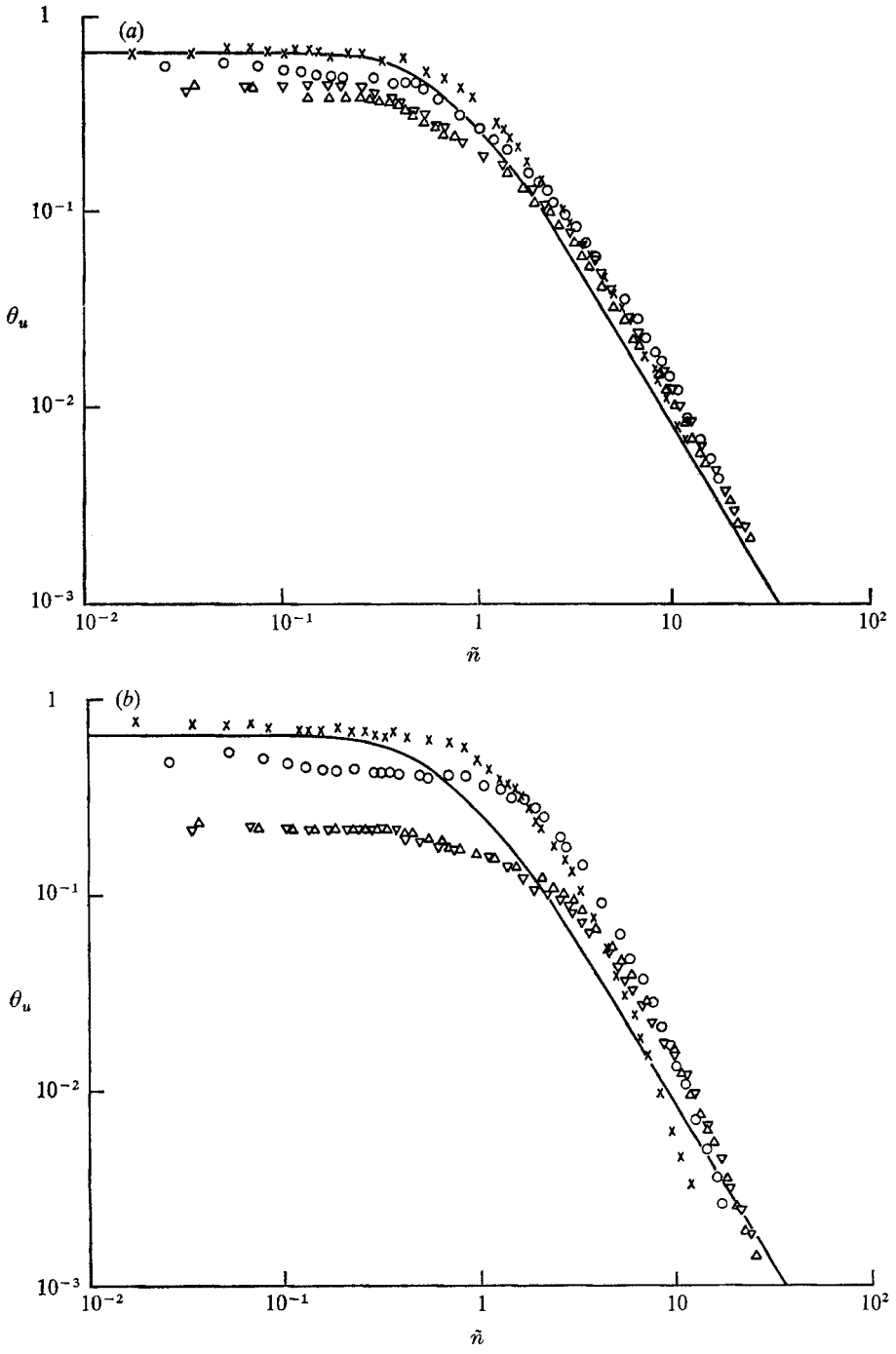

FIGURE 5. Spectra of the u component. ×, grid A; ○, grid B; △, grid C; ▽, grid D; ——, von Kármán spectrum. (*a*) $x/D = 0{\cdot}624$. (*b*) $x/D = 0{\cdot}183$.

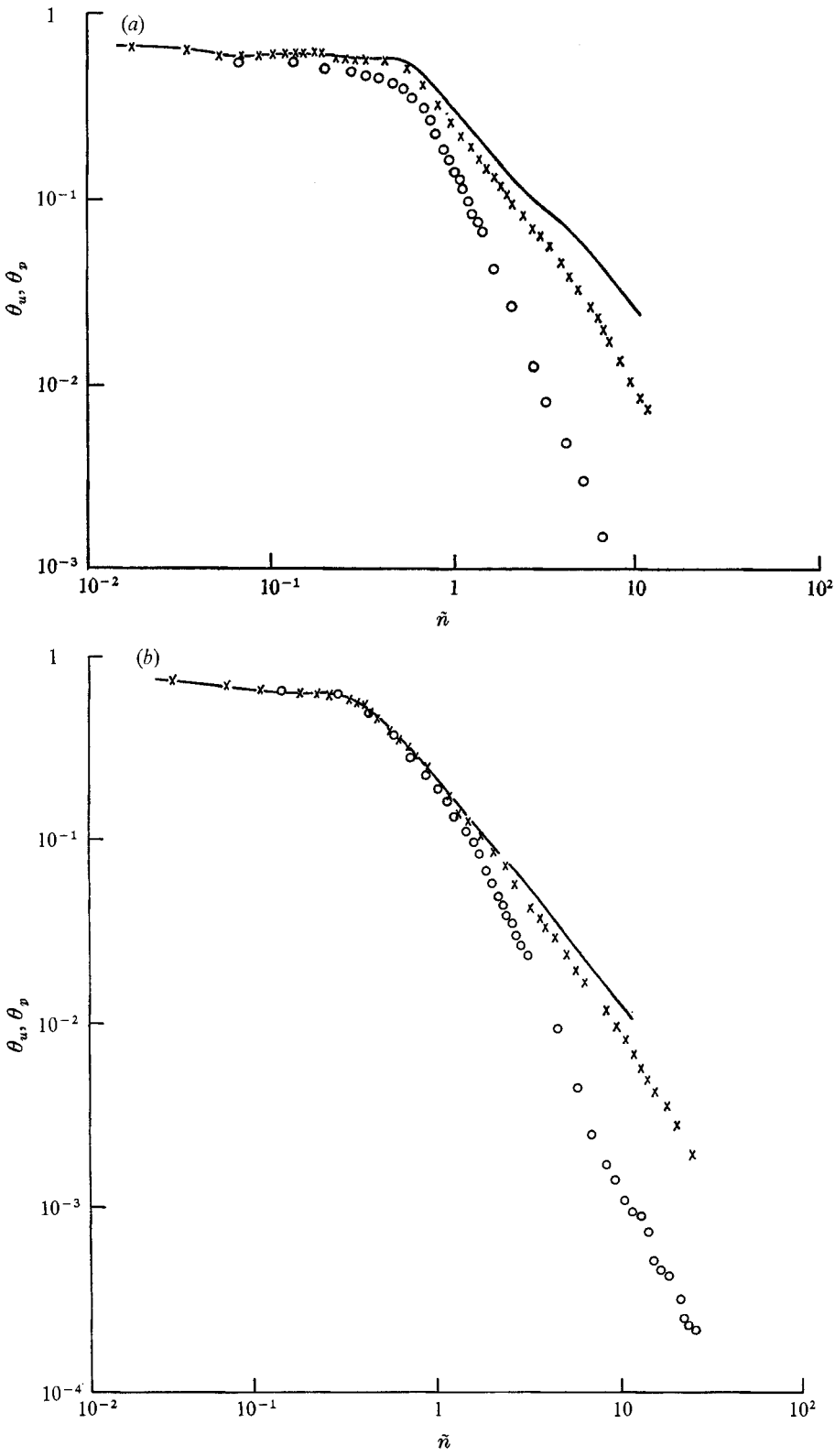

FIGURE 6. Spectrum of pressure fluctuations at the stagnation point. ○, pressure θ_p; ×, velocity θ_u; ——, equation (9) (below). (*a*) Grid *A*. (*b*) Grid *C*.

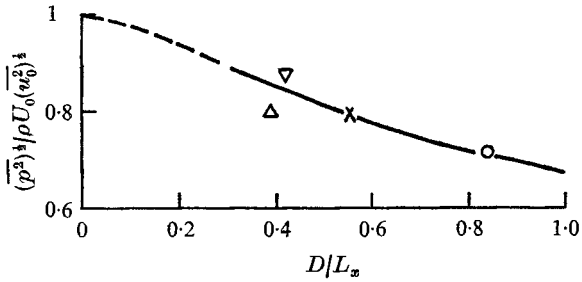

FIGURE 7. Root-mean-square value of the pressure fluctuations at the stagnation point. ○, grid A; ×, grid B; △, grid C; ▽, grid D.

Measurements of pressure fluctuations at the stagnation point

For each of the grids, power spectral density measurements of the fluctuating pressure were made, and the spectra for grids A and C, representing the smallest and largest values of L_x/D examined, are shown in figures 6 (a) and (b). The power spectral density of the pressure, $F(p)(n)$, is presented in the non-dimensional form $(F(p)(n))/(2\pi L_x \rho^2 \overline{u_0^2} U_0) = \theta_p$. The r.m.s. value of the fluctuating component of the pressure at the stagnation point, $(\overline{p^2})^{\frac{1}{2}}$, was measured for each of the grids. The results are shown in figure 7 plotted against the scale parameter D/L_x. The fluctuating pressure is presented in the non-dimensional form $(\overline{p^2})^{\frac{1}{2}}/\rho U_0(\overline{u^2})^{\frac{1}{2}}$ and the reason for this choice of parameter is left until § 4. The values of $(\overline{p^2})^{\frac{1}{2}}$ were calculated from the spectra after they had been corrected for the effects of the variations in the frequency response of the transducer.

4. Discussion of results

The modification of the turbulence by the body is fundamentally different in the two extreme cases where $L_x \gg D$ and $L_x \ll D$.

The case $L_x \gg D$

When $L_x \gg D$ the flow approximates to a slow quasi-steady variation of the direction and magnitude of the approaching velocity. Hunt (1971a) treats the flow around a circular cylinder assuming it to be inviscid and also assuming $(\overline{u_0^2})^{\frac{1}{2}} = (\overline{v_0^2})^{\frac{1}{2}} = (\overline{w_0^2})^{\frac{1}{2}} = \tau U_0$, where τ is small. In the x direction the flow is similar to that caused by a slow variation of the longitudinal velocity, and as the body is approached the fluctuating velocity will attenuate like the mean velocity. Hence

$$(U_0+u_0)/U_0 = (U+u)/U,$$

$$(\overline{u_0^2})^{\frac{1}{2}}/\overline{U}_0 = (\overline{u^2})^{\frac{1}{2}}/\overline{U}$$

and

$$(\overline{u^2})^{\frac{1}{2}}/(\overline{u_0^2})^{\frac{1}{2}} = \overline{U}/\overline{U}_0. \tag{1}$$

In the y direction the effect of v_0 will be to alter the incidence of the flow and it can easily be shown by potential-flow theory that, along the stagnation streamline,

$$(\overline{v^2})^{\frac{1}{2}}/(\overline{v_0^2})^{\frac{1}{2}} = 2 - \overline{U}/\overline{U}_0. \tag{2}$$

The component in the z direction is unaffected by the presence of the body:

$$(\overline{w^2})^{\frac{1}{2}}/(\overline{w_0^2})^{\frac{1}{2}} = 1. \tag{3}$$

For a two-dimensional flat plate in a potential flow there is no change in $(\overline{v^2})^{\frac{1}{2}}$ along the stagnation streamline, although it would be unrealistic to use this result since in the real flow there is separation at the edges. For the free-streamline model it is assumed for simplicity that, at least away from the stagnation point itself, the flow is similar to that approaching a circular cylinder. This is a very idealized picture since if the scale of turbulence is infinite the v fluctuation will induce an alternating circulation on the complete body. It can be seen from figure 1 that the model cross-section has a shape similar to that of a blunt-nosed aerofoil section. The length of the body, however, is nearly an order of magnitude longer than the largest scale of turbulence and it therefore seems reasonable to treat the complete flow as inviscid and to neglect the effect of any Kutta condition at the trailing edge. Thus when the condition $L_x \gg D$ is stated this needs to be accompanied by $L_x \ll C$, where C is the chord of the model. Equations (1), (2) and (3) are shown plotted in figures 4(*a*), (*b*) and (*c*) respectively.

The case $L_x \ll D$

If $L_x \ll D$ the distortion of the turbulence along the stagnation streamline approximates to that caused by uniform plane strain, and the results of Batchelor & Proudman (1954) can be used directly. The rapid-distortion theory of Batchelor & Proudman predicts an amplification of $(\overline{u^2})^{\frac{1}{2}}$ and $(\overline{w^2})^{\frac{1}{2}}$ and an attenuation of $(\overline{v^2})^{\frac{1}{2}}$. Their results are also shown in figure 4. When the local velocity U/U_0 is less than about 0·5 the expressions of Batchelor & Proudman reduce to the simpler forms given below:

$$(\overline{u^2})^{\frac{1}{2}}/(\overline{u_0^2})^{\frac{1}{2}} = [\tfrac{3}{4}U_0/U + \tfrac{3}{8}(U/U_0)\,(\log(4U_0/U) - \tfrac{1}{2})]^{\frac{1}{2}},$$

$$(\overline{v^2})^{\frac{1}{2}}/(\overline{v_0^2})^{\frac{1}{2}} = [\tfrac{3}{4}(U/U_0)\,(\log(4U_0/U) - 1)]^{\frac{1}{2}},$$

$$(\overline{w^2})^{\frac{1}{2}}/(\overline{w_0^2})^{\frac{1}{2}} = [\tfrac{3}{4}U_0/U - \tfrac{3}{8}(U/U_0)\,(\log(4U_0/U) - \tfrac{3}{2})]^{\frac{1}{2}}.$$

The case $L_x = O(D)$

The experimental results are seen to fall between the two limiting curves with results for smaller scales generally tending towards the $L_x/D \to 0$ curve. The largest amplification of energy occurs for the w component although there is no rate of strain in this direction. Clearly, close to the body the local intensity is rising to such a high value that the assumptions made in rapid-distortion theory cannot hold and the nonlinear terms in the vorticity equation can no longer be negligible.

Although vortex stretching amplifies $(\overline{u^2})^{\frac{1}{2}}$, close to the surface the effect of the wall on small-scale eddies will be similar to its effect on larger scale eddies further away from the stagnation point, i.e. it attenuates the fluctuations. The turbulence is thus affected on the one hand by vortex stretching and rotation and on the other by the simple blocking of the flow by the body. At intermediate scale sizes it can be expected that low wavenumbers will exhibit some of the

features of $L_x \gg D$ flows while high wavenumbers will be dominated by vortex stretching. This idea is well supported by the spectra measurements of the u component, which show a large shift of energy to higher wavenumbers as the stagnation point is approached.

Before leaving the hot-wire measurements there are one or two anomalies in the results for $(\overline{v^2})^{\frac{1}{2}}$ and $(\overline{w^2})^{\frac{1}{2}}$ which should be pointed out and which may have arisen from errors in the hot-wire response or may be genuine features of the flow. In figure 4(*b*) the larger scale turbulence shows an increase in $(\overline{v^2})^{\frac{1}{2}}$ up to about $x/D = 0{\cdot}3$ and then a decrease, presumably to zero at the stagnation point. The smallest scale turbulence (grid A), however, shows an increase between $x/D = 0{\cdot}4$ and $0{\cdot}1$. Spectra measurements would be required to establish whether this is due to some selective amplification of part of the wavenumber range. Second, in figure 4(*c*) turbulence produced by grid D shows a larger amplification than the slightly larger scale turbulence produced by grid C.

Pressure fluctuations

If $L_x \gg D$ it is possible to treat the velocity fluctuations in the vicinity of the plate as irrotational and it is assumed that the unsteady version of Bernoulli's equation can be applied:

$$\tfrac{1}{2}q^2 + \frac{P}{\rho} - \frac{\partial \phi}{\partial t} + B = F(t), \tag{4}$$

where q is the total velocity, ϕ is the velocity potential, B is the body force potential and $F(t)$ is constant throughout the flow at any instant of time. It can be shown that v and w produce no significant contribution to the fluctuating pressure at the stagnation point. The problem then reduces to that of a flat plate in a flow of varying longitudinal velocity $U(t)$. The velocity potential for a flat plate normal to a stream is $\phi(t) = \frac{1}{4}U(t)(x^2 + D^2)^{\frac{1}{2}}$, and $B = x\,dU(t)/dt$.

Substituting in (4) gives

$$\tfrac{1}{2}U(t)^2 + \frac{P}{\rho} - \frac{dU(t)}{dt}\frac{(x^2 + D^2)^{\frac{1}{2}}}{4} + x\frac{dU(t)}{dt} = F(t). \tag{5}$$

Far away from the plate, equation (5) reduces to

$$\tfrac{1}{2}U(t)_0^2 + P(t)_0/\rho = F(t), \tag{6}$$

where $P(t)_0$ is the pressure far from the plate. Batchelor (1953) has shown that in isotropic turbulence the fluctuating component of the static pressure is small and obtained the relation

$$\frac{(\overline{p_0^2})^{\frac{1}{2}}}{\rho U_0 (\overline{u_0^2})^{\frac{1}{2}}} = 0{\cdot}58\frac{(u_0^2)^{\frac{1}{2}}}{U_0}.$$

The maximum value of $(\overline{p_0^2})^{\frac{1}{2}}/\rho U_0(\overline{u_0^2})^{\frac{1}{2}}$ is $3{\cdot}7 \times 10^{-2}$, which occurs in the flow behind grid D. Since it can be shown that, at the stagnation point, $(\overline{p^2})^{\frac{1}{2}}/\rho U_0(\overline{u_0^2})^{\frac{1}{2}}$ is of order unity, neglecting the upstream fluctuating static pressure will introduce little error. On substituting (6) in (5) and neglecting second-order terms the relation for the fluctuating pressure at the stagnation point becomes

$$p = \rho\left(u_0 U_0 + \frac{D}{2}\frac{du_0}{dt}\right). \tag{7}$$

A fuller and a more physically realistic treatment by Hunt (1971*a*) shows that (7) is of the correct form but that there are further terms involving spatial derivatives of u which are as important as the temporal one. By assuming that the record of the pressure fluctuations forms part of an infinite stationary random process it is possible to rewrite (7) in terms of the power spectral densities of the pressure and the upstream velocity:

$$F(p)\,(n) = \rho^2 F(n)\, U_0^2[1 + \tfrac{1}{4}(2\pi n D/U_0)^2]. \tag{8}$$

If $F(n)$ is expressed in the non-dimensional form given earlier (by dividing by $(2\pi L_x \overline{u_0^2})/U_0)$) equation (8) becomes

$$\frac{F(p)\,(n)}{2\pi\rho^2 U_0 L_x \overline{u_0^2}} = \frac{F(n)\, U_0}{2\pi L_x \overline{u_0^2}}\left[1 + \frac{1}{4}\left(\frac{2\pi n L_x}{U_0}\right)^2\left(\frac{D}{L_x}\right)^2\right],$$

so

$$\theta_p = \theta_u[1 + \tfrac{1}{4}\tilde{n}(D/L_x)^2]. \tag{9}$$

If $D/L_x \to 0$, $\theta_p = \theta_u$ and the pressure and velocity spectra, non-dimensionalized as above, should be identical. A comparison of the spectra of pressure and velocity is shown in figures 6(*a*) and (*b*), and it can be seen that they agree closely at low wavenumbers, whereas at higher wavenumbers the pressure spectra falls away below the velocity spectra rather than showing the increase indicated by (9). At each scale size examined there was a definite break point, where the pressure spectrum diverged from the velocity spectrum, and with increasing values of L_x/D the break point moved to higher wavenumbers. At high wavenumbers the pressure spectra fell off at about 1·75 times as fast as the velocity spectra. The results of Marshall (1968) measured on a disk show a similar attenuation of the pressure spectrum. These results, therefore, show that the assumptions made in deriving (7) fail before any acceleration effects are felt. The attenuation of the pressure spectra is a direct result of the rotational nature of the turbulence and the accompanying distortion of the vorticity field. Further experiments are required to determine whether there is a corresponding reduction in the correlation of these high wavenumber pressure fluctuations over the body surface. In an attempt to predict the relationship between fluctuating drag and oncoming turbulence Vickery (1965) assumed that the correlation pattern of fluctuating pressures on the face of a bluff body is identical to the lateral correlations of the u component of the approaching turbulence. The present results suggest that in order to help to explain the magnitude of the fluctuating drag measured on square plates in turbulent flow by Bearman (1971) these high wavenumber pressure fluctuations need to be substantially better correlated than this.

If $L_x/D = \infty$ then (9) shows that

$$\theta_p = \theta_u \quad \text{and} \quad (\overline{p^2})^{\frac{1}{2}} = \rho \overline{U}_0 (u_0^2)^{\frac{1}{2}} \quad \text{or} \quad (\overline{C_P^2})^{\frac{1}{2}} = 2(u_0^2)^{\frac{1}{2}}/\overline{U}_0.$$

The measurements of $(\overline{p^2})^{\frac{1}{2}}$ are shown non-dimensionalized by $\rho \overline{U}_0 (\overline{u_0^2})^{\frac{1}{2}}$ in figure 7. The results indicate that even when $D/L_x = 1$ the root-mean-square value of the pressure fluctuations is still between 60 and 70 % of $\rho \overline{U}_0 (\overline{u_0^2})^{\frac{1}{2}}$.

5. Conclusions

When $L_x/D \gg 1$ a quasi-steady type of approach can be used and, along the mean stagnation streamline, $(\overline{u^2})^{\frac{1}{2}}$ will attenuate like the mean flow, whereas if $L_x/D \ll 1$ the turbulence is distorted by the mean flow field and $(\overline{u^2})^{\frac{1}{2}}$ will amplify owing to vortex stretching. In the experiments described here $L_x/D = O(1)$ and there is found to be a combination of these effects with attenuation of energy at low wavenumbers and amplification at high wavenumbers. The other components of turbulence are found to behave in a consistent manner with the component parallel to the stagnation line on the body, which experiences no mean rate of strain, showing only amplification. Measurements of the pressure fluctuations at the stagnation point show that at low wavenumbers the level of pressure fluctuations can be predicted by simply applying Bernoulli's equation. However at higher wavenumbers the effect of the distorting field of the body is found to reduce the level of the pressure fluctuations and the pressure spectra are found to drop off 1·75 times as fast as the spectra of the approaching turbulence.

The experiments described in this paper were carried out while the author was employed in the Aerodynamics Division of the National Physical Laboratory, Teddington, Middlesex, England.

Appendix. Free-streamline model

The profile shape of the flat-plate model was designed according to Roshko's (1954) notched hodograph method. His method requires a value to be assigned to the base pressure coefficient C_{pb}. For this model C_{pb} was chosen to be -1, thus making $k = \sqrt{2}$, where $C_{pb} = 1 - k^2$, k being the ratio of the velocity along the free streamline near separation to the free-stream velocity. Roshko's method maps the flat plate and its wake on to the positive half of the real axis of the complex-w plane with the stagnation point at the origin. The free-streamline model co-ordinates are given by

$$x_m = \frac{k^2+1}{2k}\{[w(w-1)]^{\frac{1}{2}} - \log[w^{\frac{1}{2}} + (w-1)^{\frac{1}{2}}]\},$$

$$y_m = \frac{k^2+1}{2k}\left\{\frac{\pi}{2} + \frac{1}{a}[w(a^2-w^2)]^{\frac{1}{2}} + a\tan^{-1}\left(\frac{w}{a^2-w}\right)^{\frac{1}{2}}\right\}$$

for $1 \leqslant w \leqslant a^2$, where $a = (k^2+1)/(k^2-1)$.

The width of the flat plate is given by

$$D = \frac{k^2+1}{k}\left[\frac{\pi}{2} + \frac{1}{a}(a^2-1)^{\frac{1}{2}} + a\tan^{-1}\left(\frac{1}{a^2-1}\right)^{\frac{1}{2}}\right].$$

Beyond $w = a^2$ the body is parallel sided with thickness

$$h = [(k^2+1)/2k]\,\pi[1+a].$$

The resulting profile shape is shown in figure 1.

Using the hodograph method it is possible to calculate the velocity profile along the stagnation streamline:

$$\frac{U}{U_0} = \frac{2k^2}{k^2+1}\left[\left(\frac{1}{w}+\frac{1}{a^2}\right)^{\frac{1}{2}} + \left(\frac{1}{w}+1\right)^{\frac{1}{2}}\right]^{-1},$$

where

$$x = \frac{k^2+1}{2k}\left\{w(1+w)^{\frac{1}{2}} + \log\left[(1+w)^{\frac{1}{2}}+w^{\frac{1}{2}}\right] + \frac{1}{a}\left[w(a^2+w)\right]^{\frac{1}{2}} + a\log\frac{(\overline{a^2})^{\frac{1}{2}}+w+w^{\frac{1}{2}}}{a}\right\}$$

and $0 \leqslant w \leqslant \infty$. The velocity profile is plotted in figure 3.

REFERENCES

BATCHELOR, G. K. 1953 *The Theory of Homogeneous Turbulence.* Cambridge University Press.

BATCHELOR, G. K. & PROUDMAN, I. 1954 *Quart. J. Mech. Appl. Math.* **7**, 83–103.

BEARMAN, P. W. 1971 *J. Fluid Mech.* **46**, 177–198.

HINZE, J. O. 1959 *Turbulence.* McGraw-Hill.

HUNT, J. C. R. 1971*a* A theory of turbulent flow over bodies. To be published.

HUNT, J. C. R. 1971*b* *Phil. Trans. Roy. Soc.* A **269**, 457–467.

KESTIN, J. & WOOD, R. T. 1970 *J. Fluid Mech.* **44**, 461–479.

KEUTHE, A. M., WILLMARTH, W. W. & CROCKER, G. H. 1959 *Phys. Fluids*, **2**, 714–716.

MARSHALL, R. D. 1968 Pressure fluctuation correlations near an axisymmetric stagnation point. Ph.D. thesis, Colorado State University.

PIERCY, N. A. V. & RICHARDSON, E. G. 1930 *Phil. Mag.* **9**, 1038–1040.

ROSHKO, A. 1954 *N.A.C.A. Tech. Note*, no. 3168.

SADEH, W. Z., SUTERA, S. P. & MAEDER, P. F. 1970*a* *Z. angew. Math. Phys.* **21**, 699–716.

SADEH, W. Z., SUTERA, S. P. & MAEDER, P. F. 1970*b* *Z. angew. Math. Phys.* **21**, 717–742.

SUTERA, S. P. 1965 *J. Fluid Mech.* **21**, 513–534.

SUTERA, S. P., MAEDER, P. F. & KESTIN, J. 1963 *J. Fluid Mech.* **16**, 497–520.

TOWNSEND, A. A. 1954 *Quart. J. Mech. Appl. Math.* **7**, 104–127.

TUCKER, H. J. & REYNOLDS, A. J. 1968 *J. Fluid Mech.* **32**, 657–673.

VICKERY, B. J. 1965 *Nat. Phys. Lab. Aero. Rep.* no. 1143.